JOURNAL OF SOLID STATE CHEMISTRY **141,** 418–423 (1998)
ARTICLE NO. SC987965

Crystal Structure and Electronic State of the Disordered $S=1$ System $(Li_xV_{1-x})_3BO_5$ with $x \simeq 0.3$

Masashige Onoda

Institute of Physics, University of Tsukuba, Tennodai, Tsukuba 305-8571, Japan

Received April 21, 1998; in revised form July 8, 1998; accepted July 14, 1998

The crystal structure and electronic state of the $(Li_xV_{1-x})_3BO_5$ system with $x \simeq 0.3$ have been explored through measurements of the X-ray four-circle diffraction, electron transport, and magnetization. The crystal data at 297 K show an orthorhombic structure with space group *Pbam*; $a = 9.195(1)$ Å, $b = 12.209(1)$ Å, $c = 2.9922(9)$ Å, and $Z = 4$. The structure determined with the residual factors of $R = 0.017$ and $R_w = 0.018$ for 1048 independent reflections is of a ludwigite type; Li and V atoms are located at the centers of an octahedron of oxygens with mixed occupancy, and the B atom resides in the middle of the oxygen triangles. The V–V bonded linear trimer may exist there. The variable-range-hopping-like transport and the transition from a localized state with $S \simeq 1$ to a spin-glass-like state are revealed, which are basically consistent with the structural aspect.

I. INTRODUCTION

Generally, transition-metal (TM) oxides have crystal structures formed by the linkage of rigid units such as oxygen octahedra, pyramids, or tetrahedra. The transport and magnetic properties strongly depend on the structures as well as the species of TM ions. Recently, the prototypical systems of 3*d* TM oxides have intensively been studied to extract peculiar properties originating from an electron correlation, an electron–phonon coupling, or a quantum spin-fluctuation effect (1–3).

In parallel with investigations described above, the search for new TM oxide systems has continued for a long time. For example, the inclusion of alkali, alkaline earth, or other metals into the network of TM binary oxides with the highest valences provides various nonstoichiometric ternary compounds generally called bronzes (4), which are often utilized as electrode materials. The addition of boron oxides is also expected to stabilize novel structures because of the small ionic radius and the particular B–O coordination (5), leading to interesting physical and chemical properties.

This investigation describes the crystal structure determined by means of a single-crystal X-ray diffraction for the borovanadate system $(Li_xV_{1-x})_3BO_5$ that has been synthesized for the first time, and the electronic state is revealed through transport and magnetization measurements.

II. CRYTICAL STRUCTURE

Black single crystals of $(Li_xV_{1-x})_3BO_5$ were prepared from the incongruent melt under an N_2–H_2 gas flow at 1273 K with a mixture of $LiBO_2$ (99.9% purity) and $LiVO_2$ that was made according to the procedure described in (6). Polycrystalline specimens with $x = \frac{1}{3}$ were prepared by the solid-state reaction method under an N_2–H_2 gas flow as follows: Mixtures of Li_2CO_3 (99.99% purity), B_2O_3 (99.99% purity), and $2V_2O_5$ (99.99% purity) were ground and heated at 1063 K. They were ground and pressed into pellets and then heated at the same temperature. This annealing was done several times.

X-ray four-circle diffraction measurements were carried out on a Rigaku AFC-7R diffractometer (custom-made) with graphite-monochromated Mo$K\alpha$ radiation and a 18-kW rotating-anode generator at 297 K. A crystal with dimensions $0.10 \times 0.02 \times 0.17$ mm was mounted on a glass fiber. Intensity data for the structure analysis were collected using the ω–2θ scan technique. The space group and lattice constants were determined (listed in Table 1) on the basis of the systematic absences of reflections, a statistical analysis of intensity distribution, and the successful solution and refinement of the structure. Various parameters for structure solutions and refinements are also summarized in Table 1.

The structure was solved by Patterson methods, expanded using Fourier techniques, and refined by the full-matrix least-squares calculations with anisotropic displacement parameters. Atomic scattering factors were taken from (7), and anomalous dispersion effects were included with the values of (8). Calculations at the early stage of this work were performed using the UNICS III (9) and the RADIEL (10), and those at the final stage were done with the teXsan crystallographic software package (11). A table of observed and calculated structure factors has been

0022-4596/98 $25.00

TABLE 1

Crystal Data and Summary of Intensity Measurements, Structure Solutions, and Refinements of $(Li_{0.31}V_{0.69})_3BO_5$ at 297 K

Crystal system	Orthorhombic
Space group	*Pbam* (No. 55)
Z value	4
a (Å)	9.195(1)
b (Å)	12.209(1)
c (Å)	2.9922(9)
V (Å^3)	335.91(8)
$\mu_{MoK\alpha}$ (mm^{-1})	5.987
D_{cal} (Mg/m^3)	4.016
Radiation	Mo$K\alpha$
$2\theta_{max}$ (deg)	80
Number of unique reflections	1251
R_{int}	0.010
Corrections	Lorentz-polarization Absorption (trans. factors: 0.90–1.00) Secondary extinction
Structure solution	Patterson method
Refinement	Full-matrix least-squares
Number of observations ($I > 3\sigma$)	1048
Number of variables	58
Reflection/parameter ratio	18.07
R^a	0.017
$R_w{}^b$	0.018

[a] $R = \sum||F_o| - |F_c||/\sum|F_o|$.
[b] $R_w = [\sum w(|F_o| - |F_c|)^2/\sum wF_o^2]^{1/2}$.

deposited with the National Auxiliary Publications Service (NAPS).[1]

The atomic coordinates, equivalent isotropic thermal parameters, and anisotropic displacement parameters for the crystal structure at 297 K are listed in Table 2. The unit cell contains four crystallographically independent VL sites consisting of V and Li, labeled VL1 ~ VL4, and five O sites labeled O1 ~ O5, and one B site. Here, the occupancy probabilities of V at the VL1 ~ VL4 sites are determined to be 0.952(2), 0.534(1), 0.463(1), and 0.720(1), respectively, leading to the chemical formula $(Li_{0.31}V_{0.69})_3BO_5$ with $Z = 4$, where the sum of the probabilities at each site is constrained equal to unity for simplicity. The condition of mixed occupancy is indispensable for explaining the intensity distribution of the Fourier map. A study of the phase diagram of the Li_2O–V_2O_3–B_2O_3 system under an N_2–H_2 gas flow also indicates that the single phase of $(Li_xV_{1-x})_3BO_5$ exists only at around the composition ratio Li_2O:V_2O_3:$B_2O_3 = 1:2:1$ (12), which corresponds to $x = \frac{1}{3}$ of the system. The displacement parameters of all the atoms may be normal as shown in Table 2.

The crystal structure of $(Li_{0.31}V_{0.69})_3BO_5$ projected on the orthorhombic *ab* plane is shown in Fig. 1a. Here, the large and medium-sized circles represent the O and VL atoms, respectively, with labels, and the small circle indicates the B atom. The open circle and the shaded circle show the atoms at $z = 0$ and $\frac{1}{2}$, respectively. This structure is found to be similar to that of a ludwigite Mg_2FeBO_5 with cation valences Mg^{2+}, Fe^{3+}, and B^{3+} (13, 14). Although the presence of the related compound Mg_2VBO_5 is known (15), no detailed structure determination has been performed. As previously described for a ludwigite (14), there exist two characteristic layered units, which are slanted at about 60° to the *b* direction and extend along the *c* direction: One unit consists of two "O2–O4–O1–O5" layers of hexagonally close-packed oxygen atoms and another unit is composed of two "O3–O5–O3–O4" layers and one "O1–O2–O2–O1" layer with simple square packing of oxygen atoms. These two superimposed units build up the structure. The VL1 ~ VL4 atoms are located at the centers of an octahedron of oxygens and the B atom occupies the middle of the oxygen triangles, which are familiar units for B_2O_3 (5). Figure 1b shows a clinographic view for the structure with the polyhedral scheme. Selected interatomic distances except for trivial values corresponding to the lattice constant *c* are listed in Table 3.

On the assumption that Li, B, and O ions are in the states of Li^+, B^{3+}, and O^{2-}, respectively, the average valence of V ions expected from the chemical formula is nearly trivalent. Based on the interatomic distances and the occupancy probabilities at the VL1 ~ VL4 sites, the effective ionic radii of V^{3+} and Li^+ are estimated to be 0.63 and 0.71 Å, respectively, with the radius of the oxygen ion 1.40 Å (16). The value for the V^{3+} ion is consistent with the previous report (16), but the value for Li^+ is somewhat small. From this result, the average valences at the VL1 ~ VL4 sites are found to be 2.9, 2.1, 1.9, and 2.4, respectively, which are roughly consistent with the valence distribution of a ludwigite. Namely, a ludwigite-type structure is stabilized by appropriately mixed occupancy of Li and V atoms. In a ludwigite, magnetic Fe^{3+} ions form linear chains by sharing the oxygen edges, which are separated from each other by linear chains of nonmagnetic Mg^{2+} ions. On the other hand, $(Li_{0.31}V_{0.69})_3BO_5$ may have a three-dimensional spin network as well as a significant disorder effect due to the mixed occupancy of Li and V atoms.

The VL–VL distances in Table 3 are classified into three groups; 2.74 Å, 2.99 ~ 3.11 Å, and 3.44 Å. The shortest pair exists between the VL1 and VL4 sites in the *ab* plane and this distance is much smaller than the average value in the

[1] See NAPS Document No. 05485 for 9 pages of supplementary material. This is not a multi-article document. Order from NAPS c/o Microfiche Publications, 248 Hempstead Turnpike, West Hempstead, New York, NY 11552-2664. Remit in advance in U.S. funds only $9.55 for photocopies or $5.00 for microfiche. There is a $25.00 invoicing charge on all orders filled before payment. Outside U.S. and Canada add postage of $4.50 for the first 20 pages and $1.00 for each 10 pages of material thereafter, or $1.75 for the first microfiche and $1.00 for each microfiche thereafter.

TABLE 2
Atomic Coordinates, Equivalent Isotropic Thermal Parameters B_{eq} (Å^2),[a] and Anisotropic Displacement Parameters U_{ij}[b] of $(Li_{0.31}V_{0.65})_3BO_5$ at 297 K

Atom[c]	Site	x	y	z	B_{eq}	U_{11}	U_{22}	U_{33}	U_{12}
VL1	4*h*	0.24183(3)	0.11146(2)	$\frac{1}{2}$	0.440(4)	0.00580(9)	0.00521(8)	0.00569(9)	−0.00064(8)
VL2	4*g*	0.00191(4)	0.28162(3)	0	0.449(6)	0.0046(2)	0.0055(1)	0.0070(2)	0.0002(1)
VL3	2*a*	0	0	0	0.453(10)	0.0050(2)	0.0051(2)	0.0071(3)	−0.0003(2)
VL4	2*d*	0	$\frac{1}{2}$	$\frac{1}{2}$	0.572(7)	0.0079(2)	0.0061(2)	0.0078(2)	0.0019(1)
O1	4*g*	0.1077(4)	0.14498(9)	0	0.72(2)	0.0082(4)	0.0117(4)	0.0076(5)	0.0019(4)
O2	4*g*	0.3837(1)	0.07476(8)	0	0.70(2)	0.0075(4)	0.0087(4)	0.0104(5)	0.0012(3)
O3	4*h*	0.1260(1)	0.35758(9)	$\frac{1}{2}$	0.82(2)	0.0058(4)	0.0091(4)	0.0161(5)	0.0002(4)
O4	4*h*	0.3514(1)	0.45679(8)	$\frac{1}{2}$	0.73(2)	0.0075(4)	0.0062(4)	0.0140(5)	−0.0005(3)
O5	4*h*	0.3510(1)	0.26147(8)	$\frac{1}{2}$	0.75(2)	0.0073(4)	0.0060(4)	0.0151(6)	0.0009(3)
B	4*h*	0.2756(2)	0.3595(1)	$\frac{1}{2}$	0.58(2)	0.0071(6)	0.0069(5)	0.0082(6)	0.0000(5)

[a] $B_{eq} = \frac{8}{3}\pi^2[U_{11}(aa^*)^2 + U_{22}(bb^*)^2 + U_{33}(cc^*)^2 + 2U_{12}aa^*bb^*\cos\gamma + 2U_{13}aa^*cc^*\cos\beta + 2U_{23}bb^*cc^*\cos\alpha]$.
[b] $T = \exp[-2\pi^2(a^{*2}U_{11}h^2 + b^{*22}U_{22}k^2 + c^{*2}U_{33}l^2 + 2a^*b^*U_{12}hk + 2a^*c^*U_{13}hl + 2b^*c^*U_{23}kl)]$, where $U_{13} = U_{23} = 0$ for all atoms.
[c] The VL1 ~ VL4 sites consist of V and Li, where the occupancy probabilities of V at these sites are 0.952(2), 0.534(1), 0.463(1), and 0.720(1), respectively.

spin-singlet trimerized state of the triangular $S = 1$ system $LiVO_2$ (6, 17, 18). Thus, the VL1–VL4–VL1 bonded cluster or the linear-trimer may be formed, although Li ions occupy the VL4 site in sizable probability. The distances in other groups are too large for significant direct overlap of the V 3*d* wavefunctions (19).

III. TRANSPORT AND MAGNETIC PROPERTIES

The electrical resistivity ρ for the single crystal was measured by a dc four-terminal method in the temperature region between 80 and 300 K with a current I parallel to the crystallographic c axis.

A plot of ρ versus inverse temperature (bottom abscissa) shown in Fig. 2 indicates that this compound is like a semiconductor. From the dashed line, the energy gap E_g/k defined by $\rho = \rho_0\exp(E_g/kT)$, where ρ_0 is assumed to be a constant and k is the Boltzmann constant, is estimated to be 2.4×10^3 K. Another plot (top abscissa) is based on a three-dimensional variable-range-hopping (VRH) model, $\rho = \rho_0'\exp[(T_0/T)^{1/4}]$, where ρ_0' is a constant and T_0 is equal to α^3/n. α and n represent the envelop of the wavefunction as $\exp(-\alpha r)$ and the density of states for the hopping, respectively (20). The solid line in Fig. 2 provides $T_0 = 3.7 \times 10^8$ K. Thus, when the energy range around the Fermi level for the d orbital distribution is smaller than 1 eV, the localization length α^{-1} is smaller than 10^{-1} Å, indicating a strong localization.

The magnetization of the polycrystalline specimen was measured by the Faraday method with the field of up to 1 T between 4.2 and 500 K. The magnetic susceptibility was deduced from the linear coefficient of magnetization against field (M–H) curve in the decreasing process of the field. X-ray powder diffraction patterns at 297 K for this specimen measured on a two-circle diffractometer with Cu$K\alpha$ radiation agreed well with those calculated from the atomic parameters listed in Table 2.

The temperature dependence of the inverse magnetic susceptibility χ^{-1} is shown in Fig. 3a. This has a Curie–Weiss type temperature dependence above about 100 K: $\chi = C/(T + T_W) + \chi_0$, where C, T_W, and χ_0 are, respectively, the Curie constant, Weiss temperature, and the temperature-independent contributions from the Van Vleck orbital and diamagnetic susceptibilities. The solid curve in Fig. 3a is based on the parameters $C = 1.54$ emuK/mol, $T_W = 125$ K, and $\chi_0 = 4.4 \times 10^{-4}$ emu/mol. This Curie constant is close to the free-ion value for V^{3+} with $S = 1$.

In the region below 100 K, the temperature dependence of χ^{-1} deviates from the solid curve and has a peak at around 10 K. Considering the X-ray diffraction result, this behavior is not attributed to the magnetic impurity or lattice imperfection. At temperatures below about 25 K, the remanent magnetization σ, defined by $M = \chi H + \sigma$, appears as shown in Fig. 3b. This thermal variation is different from that expected from the weak ferromagnetism, $\sigma/\sigma_0 = \tanh[\sigma T_c/(\sigma_0 T)]$, where σ_0 is the value at 0 K and T_c is the transition temperature. Two possible reasons are considered: One is the formation of short-range-ordered clusters with the antiferromagnetic correlation originating from the disorder as well as the competition of different superexchange interactions as expected from the crystal structure. The occurrence of σ is probably due to the freezing of the clusters, i.e., the transition to the spin-glass-like phase. Another reason is based on a model that the isolated linear trimer, within which the antiferromagnetic exchange coupling between adjacent V^{3+} ions is much larger than that between the two terminal V^{3+} ions, has a ground state with the total spin number $S_t = 1$ (21). In this case, the Curie

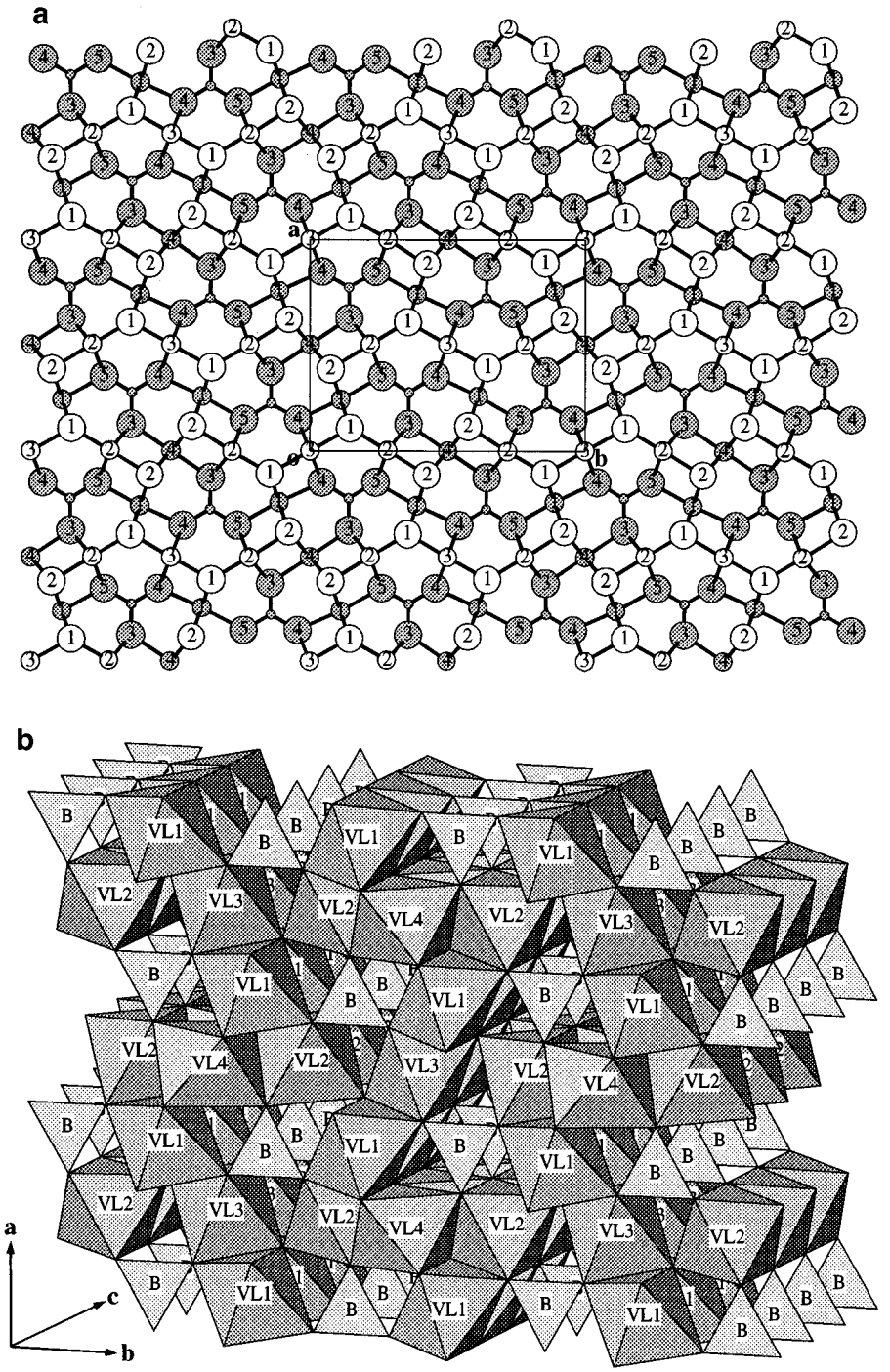

FIG. 1. The crystal structure of $(Li_{0.31}V_{0.69})_3BO_5$. (a) Projection on the orthorhombic *ab* plane, where the large and medium-sized circles represent the O and VL atoms with labels, respectively, and the small circle indicates the B atom. The open and shaded circles show the atoms at $z = 0$ and $\frac{1}{2}$, respectively. (b) Clinographic view with the $VL1O_6 \sim VL4O_6$ octahedra and the BO_3 triangles.

constant at the low-temperature limit is expected to be a third of that at the high-temperature limit, which is equal to the value estimated on the basis of a Curie–Weiss law as described earlier. This behavior is very similar to the present susceptibility result, but the occurrence of σ may not be explained by the linear trimer model alone. Since the paramagnetic contributions from V^{3+} ions that do not participate in the linear trimer should be considered, it is not easy to obtain an evidence of the linear trimer from susceptibility measurements.

TABLE 3
Selected Interatomic Distances (Å) of $(Li_{0.31}V_{0.65})_3BO_5$ at 297 K[a]

$VL1O_6$ octahedron		$VL2O_6$ octahedron		$VL3O_6$, $VL4O_6$ octahedra		BO_3 triangle, others	
VL1(i)–O1(i, ii)[b]	1.9817(7)	VL2(i)–O1(i)	1.931(1)	VL3(i)–O1(i, vii)	2.028(1)	B(i)–O3(i)	1.377(2)
–O2(i, ii)	2.0346(7)	–O2(iv)	2.063(1)	–O4(iii, iv, vi, viii)	2.0939(7)	–O4(i)	1.377(2)
–O4(iii)	2.074(1)	–O3(i, v)	2.0975(8)	O1(i)–O4(iii, viii) × 2	2.767(1)	–O5(i)	1.384(2)
–O5(i)	2.089(1)	–O5(iv, vi)	2.1070(8)	–O4(iv, vi) × 2	3.056(1)	VL1(i)–VL2(i, ii)	3.3796(5)
O1(i)–O2(i) × 2	2.678(2)	O1(i)–O3(i) × 2	3.001(1)	O4(iii)–O4(vi) × 2	2.930(2)	–VL2(xii, xiii)	3.1083(5)
–O4(iii) × 2	2.767(1)	–O5(iv) × 2	3.019(1)	VL4(i)–O2(iv, vi, ix, x)	2.0532(7)	–VL3(i, ii)	3.0058(3)
–O5(i) × 2	3.044(1)	O2(iv)–O3(i) × 2	2.808(1)	–O3(i, xi)	2.089(1)	–VL4(xiii)	2.7362(3)
O2(i)–O4(iii) × 2	2.997(1)	–O5(iv) × 2	2.743(1)	O2(iv)–O2(ix) × 2	2.812(2)	VL2(i)–VL3(i)	3.4382(5)
–O5(i) × 2	2.743(1)	O3(i)–O5(vi) × 2	2.916(2)	–O3(i) × 4	2.808(1)	–VL4(i, v)	3.0572(4)
				–O3(xi) × 4	3.046(1)		

[a] Trivial values corresponding to the lattice constant c are not listed.
[b] The translation codes are (i) x, y, z; (ii) $x, y, 1+z$; (iii) $\frac{1}{2}-x, -\frac{1}{2}+y, 1-z$; (iv) $-\frac{1}{2}+x, -\frac{1}{2}+y, 1-z$; (v) $x, y, -1+z$; (vi) $-\frac{1}{2}+x, \frac{1}{2}-y, 1-z$; (vii) $-x, -y, z$; (viii) $\frac{1}{2}-x, -\frac{1}{2}+y, -z$; (ix) $\frac{1}{2}-x, \frac{1}{2}+y, -z$; (x) $\frac{1}{2}-x, \frac{1}{2}+y, 1-z$; (xi) $-x, 1-y, z$; (xii) $\frac{1}{2}+x, \frac{1}{2}-y, -z$; (xiii) $\frac{1}{2}+x, \frac{1}{2}-y, 1-z$.

IV. CONCLUSION

The crystal structure of the $(Li_xV_{1-x})_3BO_5$ system with $x \simeq 0.3$ is of a ludwigite-type and is built up of two layered units with hcp and square-packed oxygen atoms. This is also viewed as a linkage of (Li, V)O_6 octahedra and BO_3 triangle. The existence of the V–V-bonded linear trimer has been proved from structural viewpoints. The electronic states are characterized by the variable-range-hopping-like transport and the transition from a localized state of V^{3+} ions with $S \simeq 1$ to a spin-glass-like state, which are basically consistent with the structural aspect.

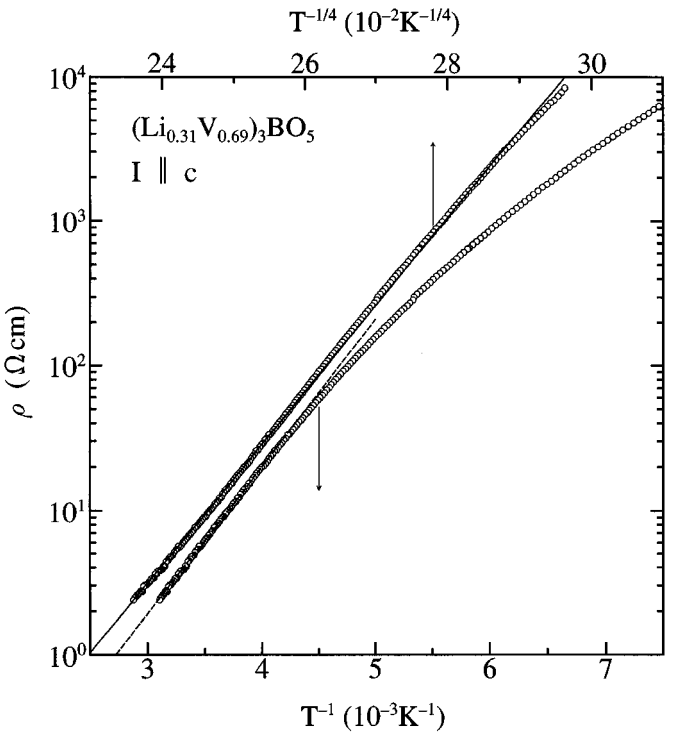

FIG. 2. The temperature dependence of the electrical resistivity ρ of $(Li_{0.31}V_{0.69})_3BO_5$ with a current I parallel to the c-axis. The dashed and solid lines show the results calculated on the basis of a semiconductor model (bottom abscissa) and a three-dimensional variable-range-hopping model (top abscissa), respectively.

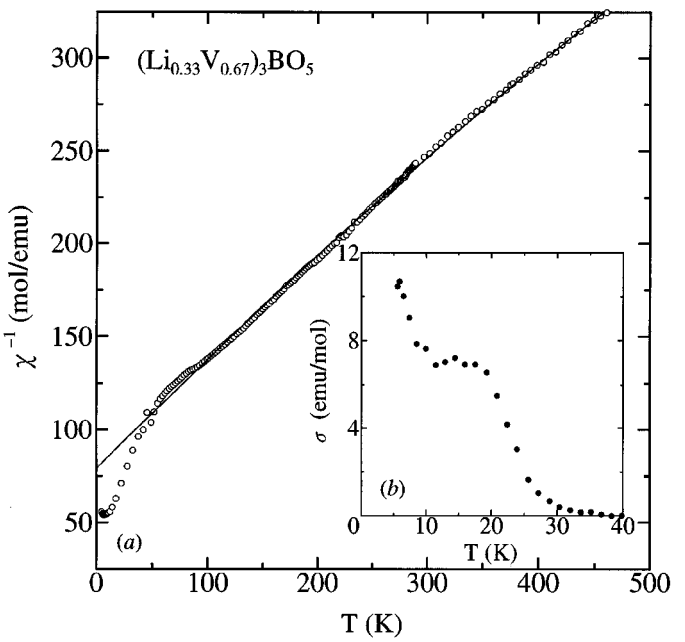

FIG. 3. The temperature dependences of (a) the inverse magnetic susceptibility χ^{-1} and (b) the remanent magnetization σ of $(Li_{0.33}V_{0.67})_3BO_5$, where the solid curve indicates the results calculated on the basis of a Curie–Weiss law.

Unfortunately, the present susceptibility results do not provide specific information on magnetic properties of the linear trimer owing to considerable amount of V^{3+} ions that do not participate in this bound state. To further describe the electronic state of this system, NMR measurements for entire nuclei are in progress.

A comparison between the valence states for $(Li_{0.31}V_{0.69})_3BO_5$ and Mg_2FeBO_5 indicates that the present system is stabilized by appropriate tuning of ionic radii and valences of cations. Therefore, characteristic spin networks such as one-dimensional chains and ladders could be constructed by controlling a kind of cations, which will give new physical insights for quantum spin-fluctuation effects.

ACKNOWLEDGMENT

N. Fukushima is gratefully acknowledged for his help in magnetic measurements.

REFERENCES

1. N. F. Mott, "Metal–Insulator Transitions," 2nd ed., Taylor & Francis, London, 1990.
2. A. Georges, G. Kotliar, W. Krauth, and M. Rozenberg, *Rev. Mod. Phys.* **68,** 13 (1996).
3. E. Dagotto and T. M. Rice, *Science* **271,** 618 (1996).
4. For example, J. Galy, *J. Solid State Chem.* **100,** 229 (1992).
5. S. V. Berger, *Acta Chem. Scand.* **7,** 611 (1953).
6. M. Onoda, T. Naka, and H. Nagasawa, *J. Phys. Soc. Jpn.* **60,** 2550 (1992).
7. D. T. Cromer and J. T. Waber, *in* "International Tables for X-Ray Crystallography" (J. A. Ibers and W. C. Hamilton, Eds.), Vol. IV, Sect. 2, Kynoch Press, Birmingham, 1974.
8. D. C. Creagh and W. J. McAuley, *in* "International Tables for Crystallography" (A. J. C. Wilson, Ed.), Vol. C, Kluwer Academic, Boston, 1992.
9. T. Sakurai and K. Kobayashi, *Rikagaku Kenkyusho Hokoku* **55,** 69 (1979). [In Japanese]
10. P. Coppens, T. N. Guru Row, P. Leung, E. D. Stevens, P. J. Becker, and Y. W. Yang, *Acta Crystallogr. Sect. A* **35,** 63 (1979).
11. teXsan, "Crystal Structure Analysis Package," Molecular Structure Corp., The Woodlands, TX, 1992.
12. M. Onoda, A. Honzawa, and N. Fukushima, unpublished results.
13. E. F. Bertaut, *Acta Crystallogr.* **3,** 473 (1950).
14. Y. Takeuchi, T. Watanabe, and T. Ito, *Acta Crystallogr.* **3,** 98 (1950).
15. P. Blum and H. Bozon, *Comp. Rend.* **238,** 811 (1954).
16. R. D. Shannon, *Acta Crystallogr. Sect. A* **32,** 751 (1976).
17. M. Onoda and T. Inabe. *J. Phys. Soc. Jpn.* **62,** 2216 (1993).
18. M. Onoda and H. Nagasawa, *Butsuri* **49,** 559 (1994). [In Japanese]
19. J. B. Goodenough, *Czech. J. Phys. B* **17,** 304 (1967).
20. W. Brenig, G. H. Döhler, and P. Wölfle, *Z. Phys.* **258,** 381 (1973).
21. E. König and G. König, *in* "Magnetic Properties of Coordination and Organometallic Transition Metal Compounds" (K.-H. Hellwege and A. M. Hellwege, Eds.), Landolt–Börnstein, New Series, Group II, Vol. 12, Chap. 1, Springer-Verlag, Berlin, 1984.